Electronic Supporting Information

Lead Chlorine Cluster Assembled One-dimensional Halide with Highly Efficient Broadband White-light Emission

Jian-Qiang Zhao,[a] Chen Sun,[a,b] Meng Yue,[a] Yan Meng,[a] Xian-Mei Zhao,[a] Le-Ran Zeng,[a] Guang Chen,[b,c] Cheng-Yang Yue,[a]* Xiao-Wu Lei [a]*

[a] Department of Chemistry and Chemical Engineering, Jining University, Qufu, Shandong, 273155, P. R. China

[b] College of Chemistry and Chemical Engineering, Qufu Normal University, Qufu, Shandong, 273165, P. R. China

[c] Laboratory of Tibetan Medicine Research & Qinghai Key Laboratory of Qinghai-Tibet Plateau Biological Resources, Northwest Institute of Plateau Biology, Chinese Academy of Science, Xining 810001, China

*Corresponding author: Cheng-Yang Yue, Xiao-Wu Lei

E-mail address: yuechengyang@126.com; xwlei_jnu@163.com

Experimental Section

Materials. The chemical materials and regents were commercially purchased from Aladdin chemical company and directly used in the preparation reaction without any further purification or other physical process. N,N'-Bis(3-aminopropyl)-ethylenediamine (BAPrEDA, 97%), N-Methylformamide (NMF, 99%), N,N'-Dimethylacetamide (DMA, 99%), hydrochloric acid (HCl, 37%), methanol (MeOH, AR), ethyl acetate (EA, AR) and ethanol (EtOH, AR).

Synthesis of compound [DTHPE]$_2$Pb$_3$Cl$_{10}$. Single crystals of [DTHPE]$_2$Pb$_3$Cl$_{10}$ were prepared by using a facile solvothermal reaction. The mixture of PbCl$_2$ (0.4 mmol, 0.1112 g) and BAPrEDA (0.7 mmol, 0.125 g) was dissolved in a mixed solution of EtOH (1 mL), NMF (1 mL), DMA (3 mL) and hydrochloric acid (0.25 mL). The suspension was constantly stirred about half an hour and then transfer into a 25 mL glass vial, which was then sealed and heated at constant temperature of 100 °C at least five days. After the reaction, lots of colorless block-shaped crystals were filtrated from the vial and washed with ethanol three times (yield: 53%). The structure was subsequently determined to be C$_{20}$N$_8$H$_{44}$Pb$_3$Cl$_{10}$ by using the single crystal X-ray diffraction. Elemental analysis calculated for C$_{20}$N$_8$H$_{44}$Pb$_3$Cl$_{10}$: C, 17.50 %; N, 8.16 %; H, 3.23 %; found: C, 17.42 %; N, 8.25 %; H, 3.39 %.

Herein, it should be noted that the DTHPE molecules were in *in-situ* synthesized possibly through the following reaction steps (Scheme S1). Under solvothermal conditions, NMF molecule was easily hydrolyzed to generate formic acid at higher temperature. Then, the nucleophilic substitution reactions between two terminal amino-groups of BAPrEDA (**1**) and formic acids generate intermediate product of (**2**). Finally, the internal nucleophilic substitution reactions in (**2**)

lead to the final DTHPE molecule (**3**). Of course, the terminal and internal nucleophilic substitution

reactions on all amino-groups in BAPrEDA maybe simultaneously happen to produce the DTHPE

molecules.
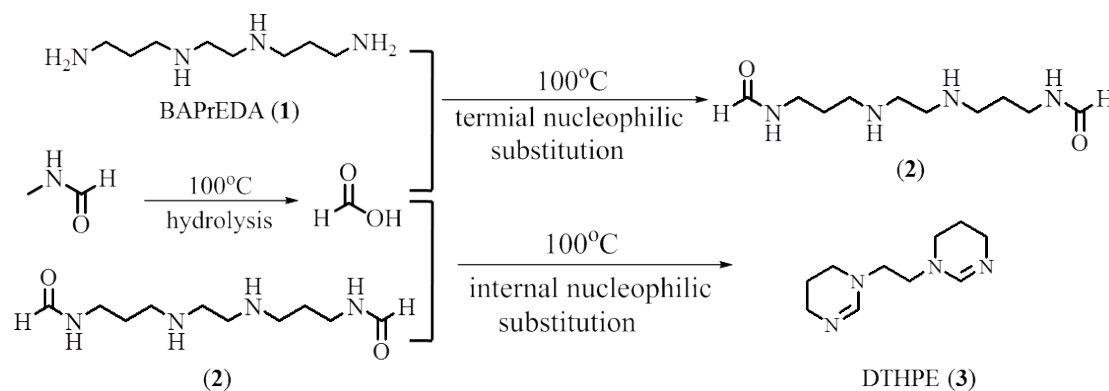
Scheme S1. The possible generation route of DTHPE molecule in the preparation process of

compound [DTHPE]$_2$Pb$_3$Cl$_{10}$.

  Synthesis of DTHPE. The synthesis of DTHPE is similar to the synthesis of compound

[DTHPE]$_2$Pb$_3$Cl$_{10}$ except no metal salt and acid. BAPrEDA (7 mmol, 1.25 g) was dissolved in a

mixed solution of EtOH (2 mL), NMF (2 mL) and DMA (6 mL). The mixed solution was

constantly stirred and then transfer into a 25 mL glass vial, which was then sealed and heated at

constant temperature of 100 °C at five days. After the reaction, The solvent was removed under

vacuum directly and the crude product was then washed with EA. The pure compound DTHPE was

obtained by multiple recrystallizations in MeOH-EA solution. Yield 41%, 0.56 g; white solid. **^{1}H**

NMR (400 MHz, D$_2$O) δ 7.98 (s, 2H), 3.73 (s, 4H), 3.47 (t, J = 5.6 Hz, 4H), 3.33 (t, J = 5.6 Hz, 4H),

2.04-1.98 (m, 4H) (Fig. S14); **^{13}C NMR** (100 MHz, D$_2$O) δ 152.8, 51.7, 43.8, 37.0, 17.8. **HRMS**

(ESI+) exact mass calculated for [M+H]$^+$ (C$_{10}$H$_{19}$N$_4$): 195.161, found: 195.160; [M+H$_3$O]$^+$

(C$_{10}$H$_{21}$N$_4$O): 213.172, found: 213.171 (Fig. S15).

Basic characterizations. The powder X-ray diffraction (XRD) of sample was performed on a Bruker D8 Advance X-ray powder diffraction meter equipped with Cu-K_α radiation ($\lambda = 1.5418$ Å). The operation of X-ray diffraction was carried out at 40 kV and 40 mA. The diffraction pattern was scanned over the angular range of 5-60 degree with a step size of 0.02 at room temperature. The simulated XRD pattern was fitted from the crystallographic information file (CIF) of single-crystal X-ray diffraction by using the Mercury software. The solid-state ultraviolet-visible (UV-Vis) optical absorption spectrum was performed on a PE Lambda 900 UV/Vis spectrophotometer spanning the whole UV-Vis light range of 200-800 nm. The thermal stability was tested by using the thermogravimetric analysis (TGA), which was carried out on a Mettler TGA/SDTA 851 thermal analyzer in the temperature range of 30-800 °C under the constant protection of nitrogen atmosphere flow. Elemental analyses of C, N and H were carried out on a PE2400 II elemental analyzer. The ^{1}H, ^{13}C NMR spectroscopic data were recorded on Bruker Mercury Plus 400 MHz NMR spectrometers. Chemical shifts (δ) for ^{1}H and ^{13}C are referenced to internal solvent resonances. ^{1}H NMR coupling constants were reported in Hz, and multiplicity was indicated as follows: s (singlet); d (doublet); t (triplet); m (multiplet). Fourier transform infrared (FT-IR) spectra were recorded from KBr pellets containing 1% of the compound in the range of 400~4000 cm^{-1} on a Nicolet Magna 750 FT-IR spectrometer. ESI-MS measurements were conducted with a Thermo Exactive spectrometer in positive and negative ion modes at a capillary temperature of 275 ºC. The spectrometer was previously calibrated with the standard tune mix to give a precision of around 2 ppm in the m/z range of 150–500.

Single crystal X-ray diffraction. The single crystal of [DTHPE]$_2$Pb$_3$Cl$_{10}$ was selected under the optical microscope and used to perform X-ray diffraction. The single crystal data was collected on

the Bruker Apex II CCD diffractometer with Mo Kα radiation ($\lambda = 0.71073$ Å) at room temperature. The crystal structure was solved by direct method and refined based on F^2 using SHELXTL-97 program.[1] All the non-hydrogen atoms were refined with anisotropic thermal parameters, and hydrogen atoms of organic molecules were positioned geometrically and refined isotropically. Structural refinement parameters of [DTHPE]$_2$Pb$_3$Cl$_{10}$ are summarized in Table S5 and important bond lengths are listed in Table S6-S8.

Photoluminescent property characterizations. The PL spectra were performed on an Edinbergh FLS980 fluorescence spectrometer. The photoluminescence quantum efficiency (PLQE) was achieved by incorporating an integrating sphere into the FLS980 spectrofluorometer. The PLQE was calculated based on the equation: $\eta_{QE} = I_S/(E_R-E_S)$, which I_S represents the luminescence emission spectrum of the sample, E_R is the spectrum of the excitation light from the empty integrated sphere (without the sample), and E_S is the excitation spectrum for exciting the sample. The time-resolved decay data were carried out using the Edinburgh FLS980 fluorescence spectrometer with a picosecond pulsed diode laser. The average lifetime was obtained by exponential fitting. The power-dependent photoluminescence spectra were measured using the 375 nm (LE-LS-375-140TFCA, 1-140 mW). The CIE chromaticity coordinates and CRI were calculated using the CIE calculator software based on the emission spectrum.

Raman measurement. The Raman measurement was performed on powders of [DTHPE]$_2$Pb$_3$Cl$_{10}$ in the range of 0-3500 cm^{-1} by using Horiba Scientific LabRam HR Evolution under 532 nm excitation wavelength.

Fabrication of white LED lamp. The well grinded powders of sample were firstly dispersed in the solution of ethyl acetate via constant ultrasonication treatment over at least 60 minutes. Then the suspension was carefully coated on one UV LED for 5-6 times until a uniform and thin film was formed on the surface of the LED. Under the same conditions, this assembly process can be repeatedly fabricated with the same technique.

Theoretical band calculation. The single crystal data of $[DTHPE]_2Pb_3Cl_{10}$ was directly used to calculate the electronic band structure in Castep software. The total energy was calculated with density functional theory (DFT) using Perdew−Burke−Ernzerhof (PBE) generalized gradient approximation.[2] The interactions between the ionic cores and the electrons were described by the norm-conserving pseudopotential. Hence, the $C-2s^22p^2$, $N-2s^22p^3$, $H-1s^1$, $Pb-6s^26p^2$ and $Cl-3s^2sp^5$ orbital were adopted as valence electrons. The number of plane wave included in the basis sets was determined by a cutoff energy of 320 eV and numerical integration of the Brillouin zone is performed using Monkhorst-Pack k-point sampling of 2×2×2. Other calculating parameters and convergence criteria were set by the default values of the CASTEP code.
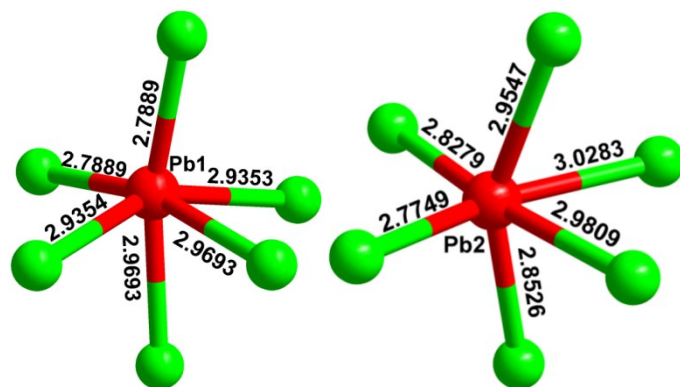
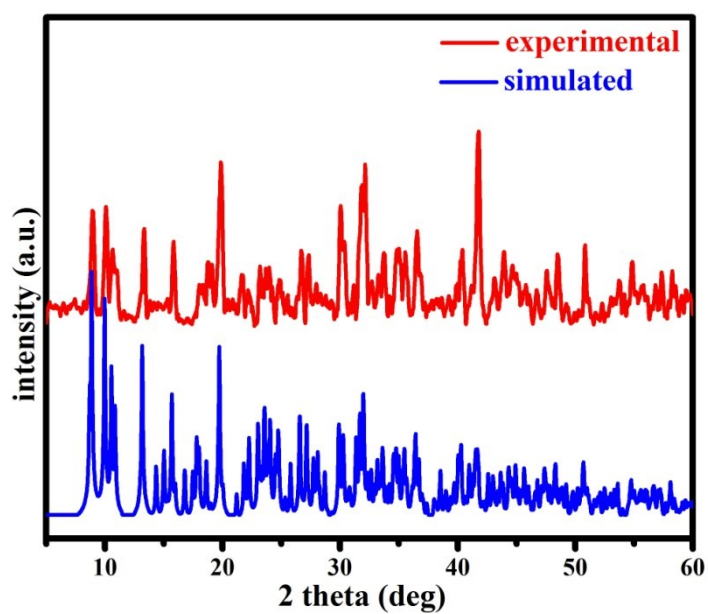**Fig. S1** The coordination environments of Pb(1) and Pb(2) atoms in the structure of [DTHPE]$_2$Pb$_3$Cl$_{10}$.

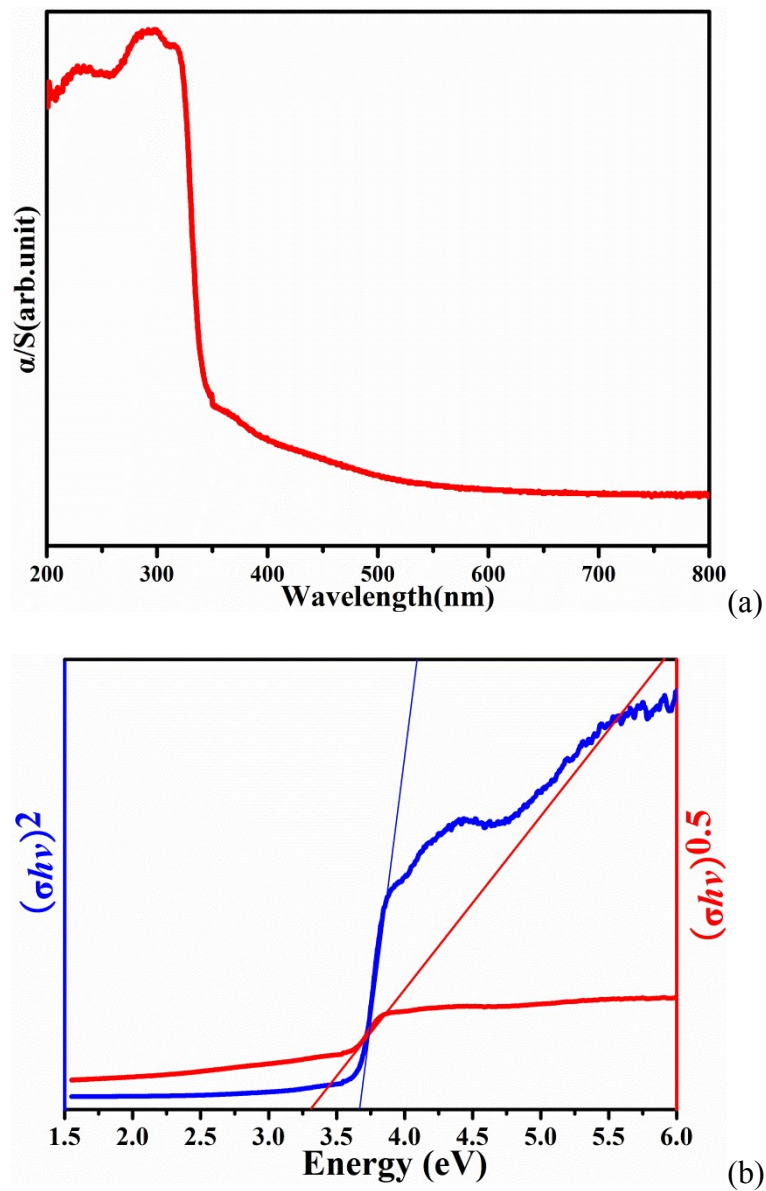**Fig. S2** The simulated and experimental XRD patterns of compound [DTHPE]$_2$Pb$_3$Cl$_{10}$.

Fig. S3 (a) the solid state UV-Vis optical absorption spectrum of compound $[DTHPE]_2Pb_3Cl_{10}$, (b) the Tauc's plots based on the assumptions of direct and indirect transitions.

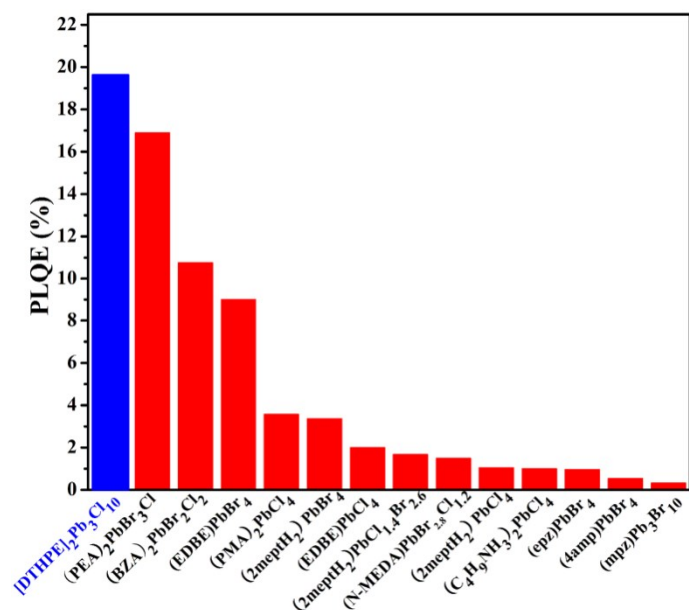**Fig. S4**. Comparison of PLQEs for [DTHPE]$_2$Pb$_3$Cl$_{10}$ and reported 2D perovskites.
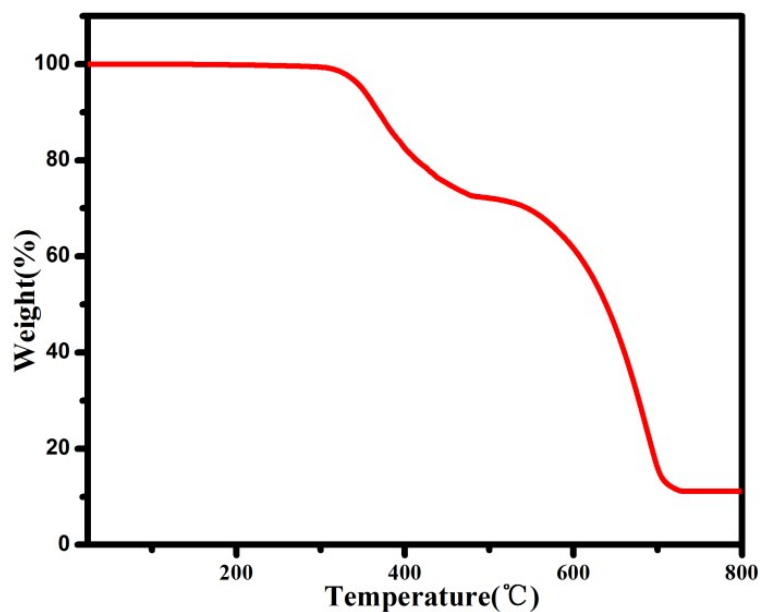

Fig. S5. The thermogravimetric analysis (TGA) curve of compound [DTHPE]$_2$Pb$_3$Cl$_{10}$. The TGA curve shows the higher thermal stability up to about 300 °C without obvious decomposition.
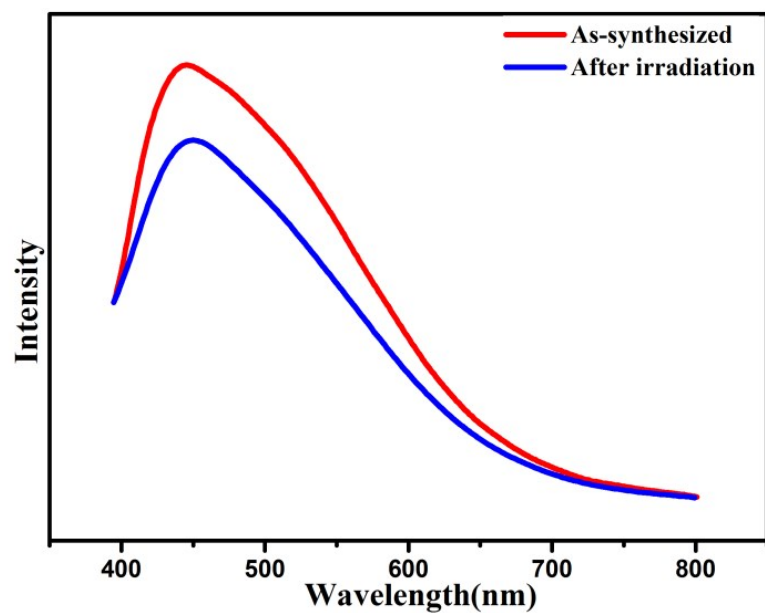
Fig. S6 Comparison of the emission spectra of as-synthesized (red line) and after irradiation under UV light for 12 hours (blue line) over compound $[DTHPE]_2Pb_3Cl_{10}$.
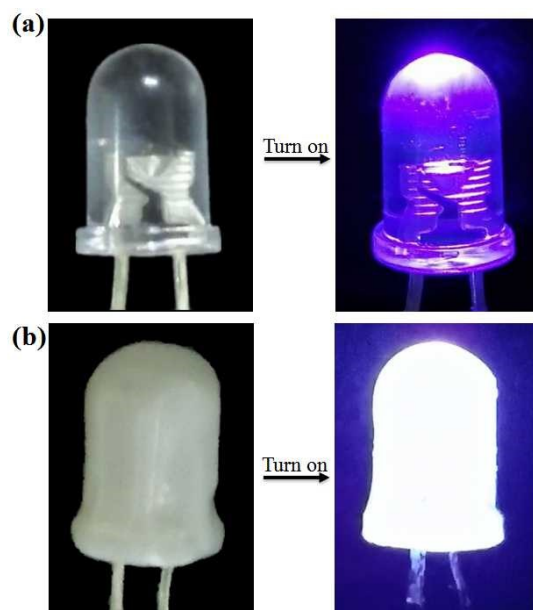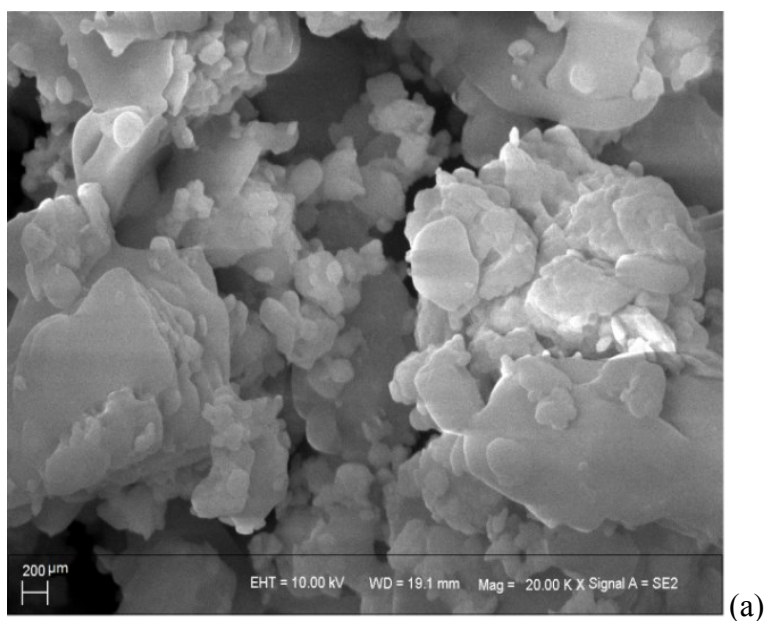
Fig. S7. (a) The photographs of commercial UV-LED lamp (left: off, right: on) and (b) The photographs of UV-LED lamp coated with a thin layer of sample [DTHPE]$_2$Pb$_3$Cl$_{10}$ (left: off, right: on).

(a)

(b)
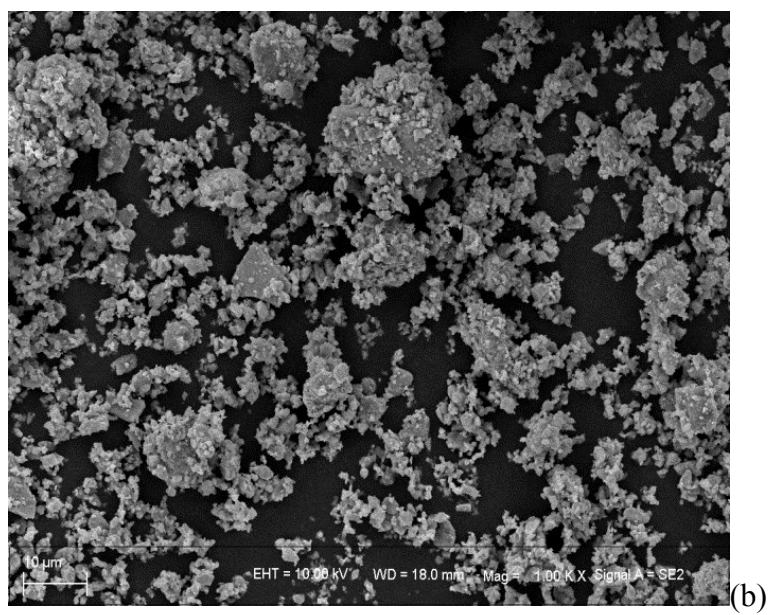
Fig. S8 SEM photo images of bulk crystals (a) and microscale crystals (b) of [DTHPE]$_2$Pb$_3$Cl$_{10}$.
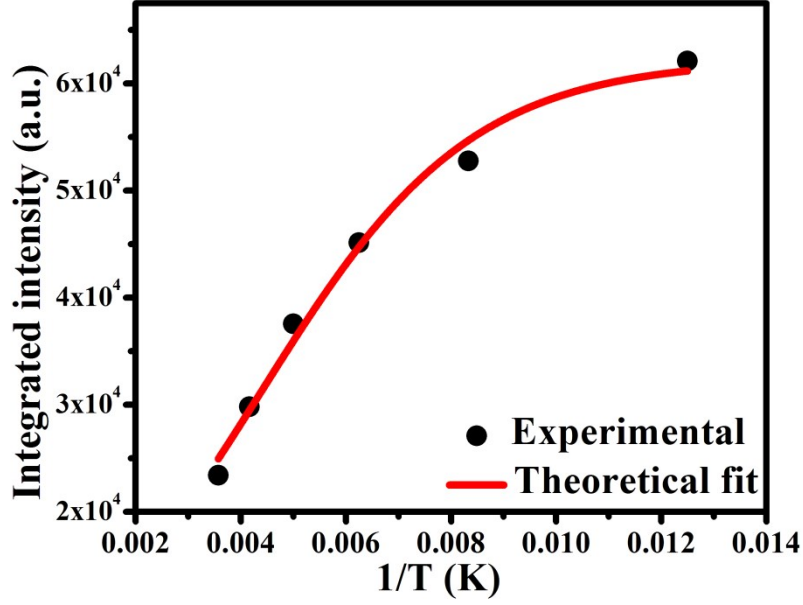
Fig. S9 Integrated PL intensity as a function of reciprocal temperature from 80 to 280 K. The thermal activation energy can be calculated from the fitting of temperature-dependent emission intensity according to the famous Arrhenius-type model:

$$I_{PL} = \frac{I_0}{1 + a \exp(\frac{-E_a}{k_B T})}$$

where I_{PL} represent the PL intensity at temperature T, I_0 is low-temperature PL intensity, K_B represent the Boltzmann constant, E_a is the activation energy and a is the ratio between the radiative and the nonradiative decay rates. The best fitting gives an activation energy (E_a) of 43.17±5.89 meV.
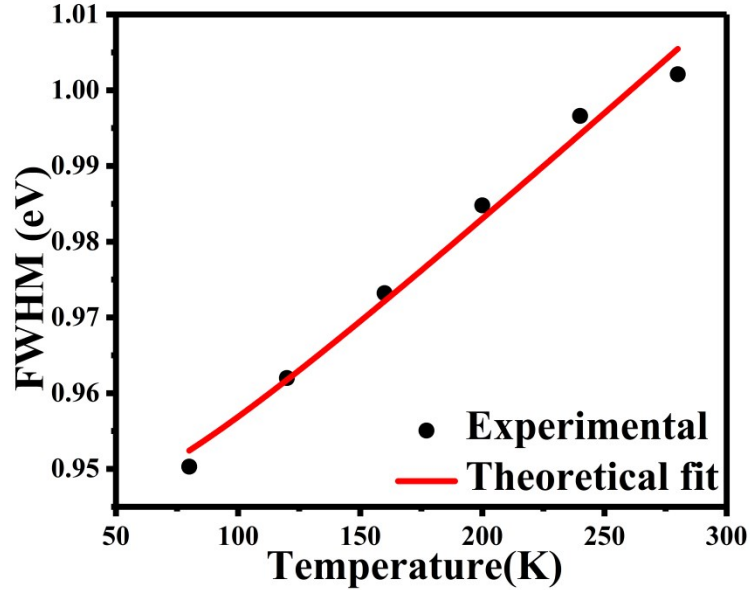
Fig. S10 The experimental and fitted temperature-dependent FWHM. The temperature-dependent FWHM can be used to estimate the electron-phonon coupling according to the follow equation:

$$\Gamma(T) = \Gamma_0 + \Gamma_{phonon}(e^{E_{LO}/k_B T} - 1)^{-1} + \Gamma_{inhomo}e^{-E_b/k_B T}$$

where Γ_0 is the FWHM of 0 K, E_{LO} represents the energy of the longitudinal-optical phonon, E_b is the average binding energy of the trap states, Γ_{phonon} and Γ_{inhomo} represent the relative contributions of electron-phonon coupling and trapped states induced inhomogeneous broadening, respectively. The best fit to the experimental data gives Γ_0 = 945.27 meV, Γ_{phonon} = 47.33 meV, Γ_{inhomo} = 159 meV, E_{LO} = 13.86 meV and E_b = 13.91 meV.

Fig. S11 Raman spectrum of compound [DTHPE]$_2$Pb$_3$Cl$_{10}$.
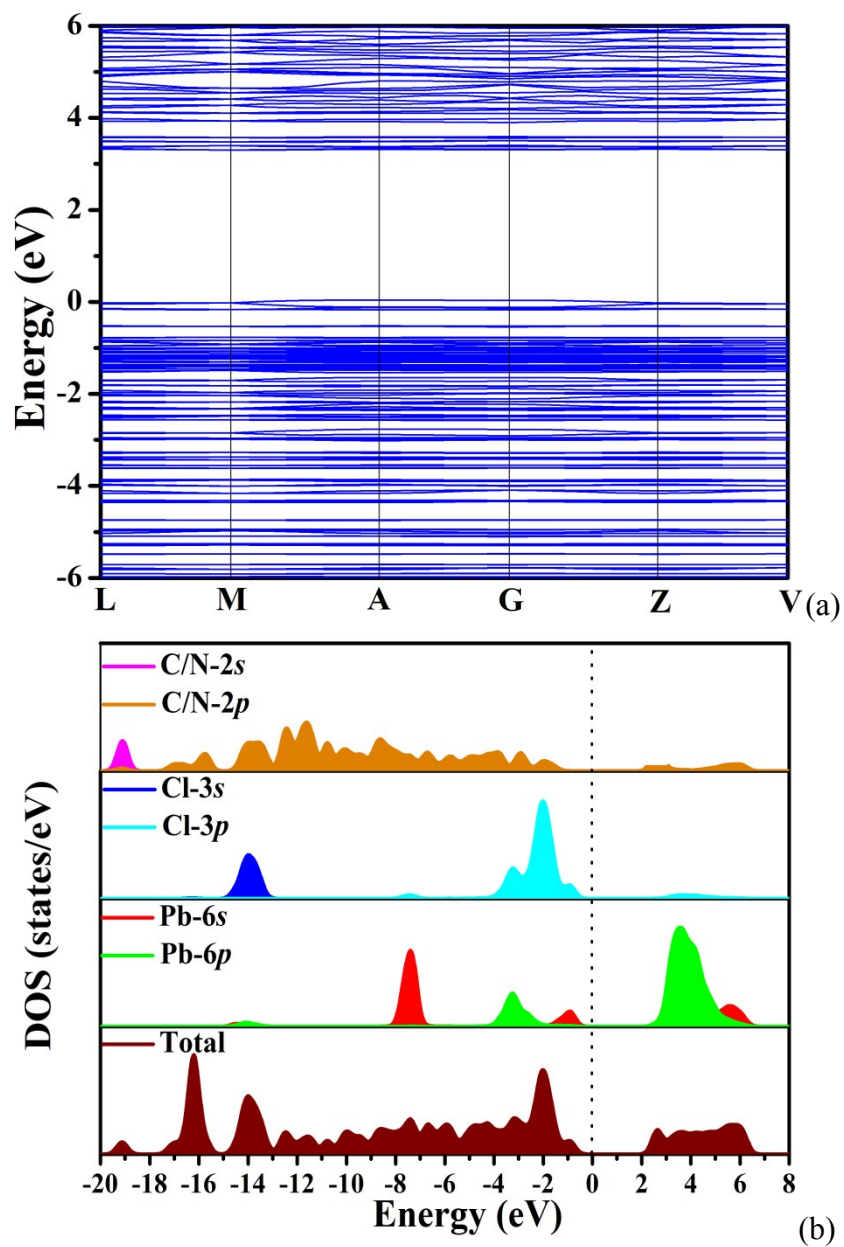
Fig. S12 The calculated electronic band structure (a) and density of states (b) for [DTHPE]$_2$Pb$_3$Cl$_{10}$.
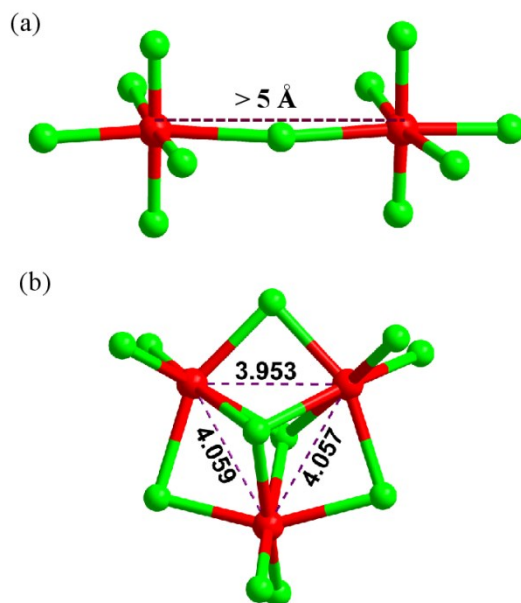
Fig. S13 Comparison of the Pb⋯Pb distances of corner-shared [PbCl$_6$] octahedrons in 2D perovskite (a) and face-shared [PbCl$_6$] octahedrons in [Pb$_3$Cl$_{11}$] cluster (b).

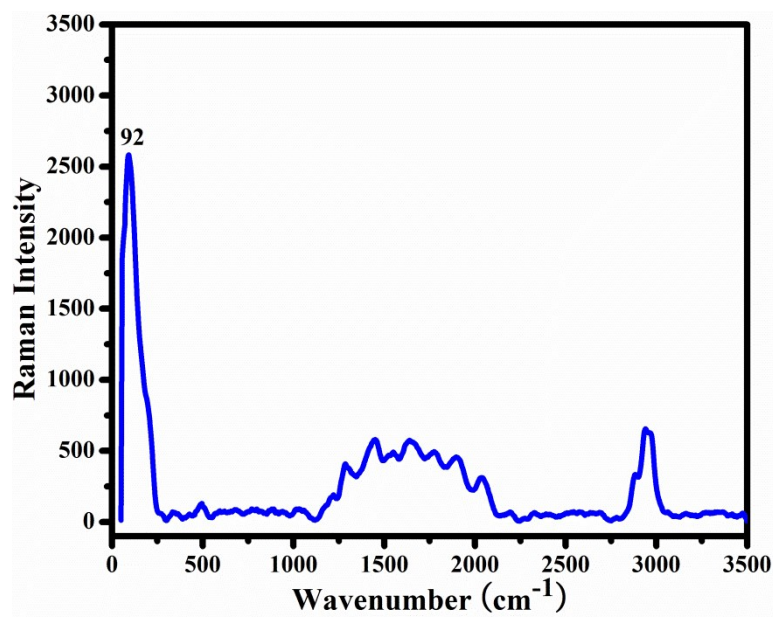**Note.** The specific crystal structure and PL mechanism facilitate us to better understand the origin of the enhanced white light emission intensity of [DTHPE]$_2$Pb$_3$Cl$_{10}$ versus corner-shared 2D perovskites based on detailed analysis of structure-property relationship. Although all the Pb atoms adopt the same octahedral coordination environments in hybrid halides, the distinct connecting manners of [PbX$_6$] octahedrons play different roles in the formation of some radiative species including Pb$_2^{3+}$ or Pb^{3+}, etc, which is positively related to the generation of STEs and broadband light emission. In the corner-shared [PbX$_6$] octahedrons, the halogens locate between the adjacent Pb atoms leading to longer Pb⋯Pb distances (> 5 Å) and weak electron interactions, which bring the difficulty to form these radiative species upon photo excitation (Fig. S13a). Although the structural distortions of 2D layers assist the shortening of Pb⋯Pb distance, such distortion extent is limited due to the steric forces of inserted halogens. Comparatively speaking, the face-shared [PbX$_6$] octahedrons in [Pb$_3$Cl$_{11}$]$^{5-}$ cluster result in higher octahedral distortion level with shorter Pb⋯Pb

distances (< 4.1 Å), which more easily facilitate the formation of radiative species and enhance the broadband light emission intensity (Fig. S13b). On the other hand, previous studies indicated that the structural dimensionality of inorganic skeleton also play an important role in the quantum confinement and lattice deformation upon photo excitation. In general, lower dimensional inorganic lattice easily generates stronger white emission with approximate follow of 1D > 2D > 3D metal halides due to stronger quantum confinement effect as well as more soft and deformable crystal lattice. Overall, the synergistic effects including higher distortion level of face-shared octahedrons, stronger quantum confinement and larger structural deformability of corner-shared 1D chain lead to more efficient white-light emission exceeding the typical 2D layered perovskites.

(a)

(b)
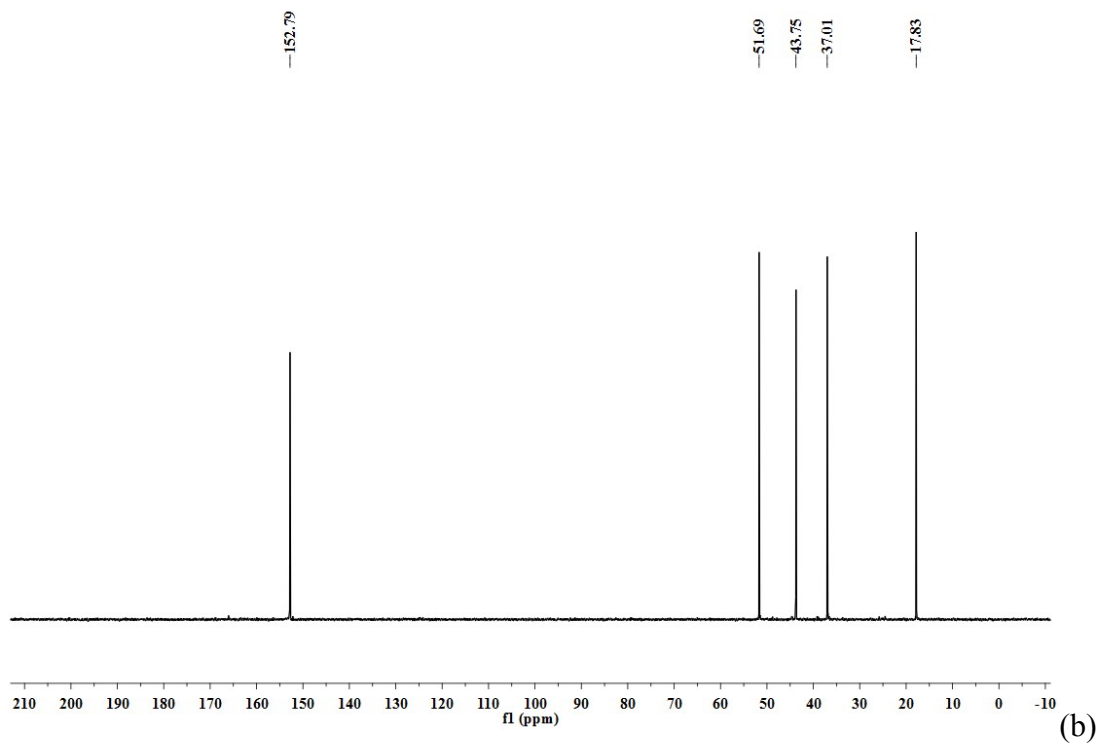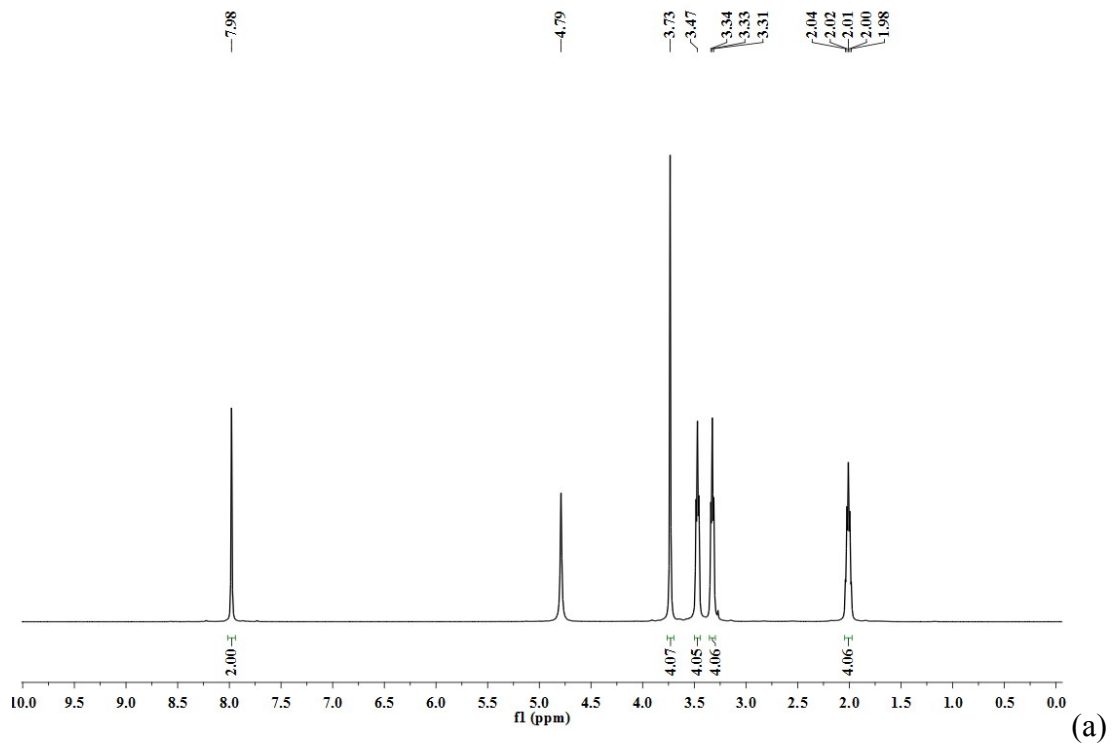
Fig. S14 The ^1H NMR spectra (a) and ^{13}C NMR spectra (b) of DTHPE.
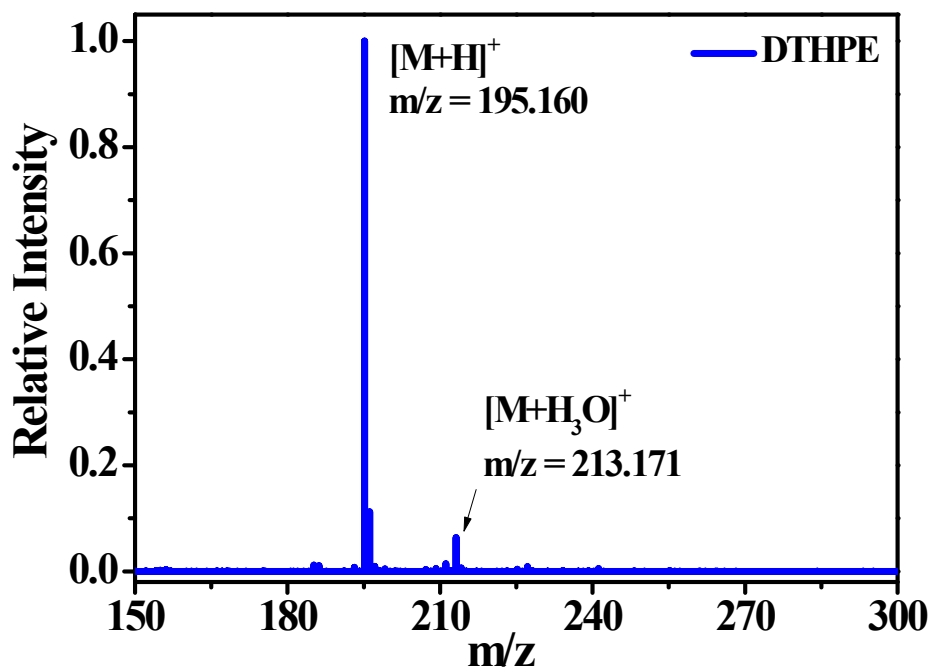
Fig. S15 The ESI-MS spectra of DTHPE in CH$_3$OH (In-Source CID 0 eV).
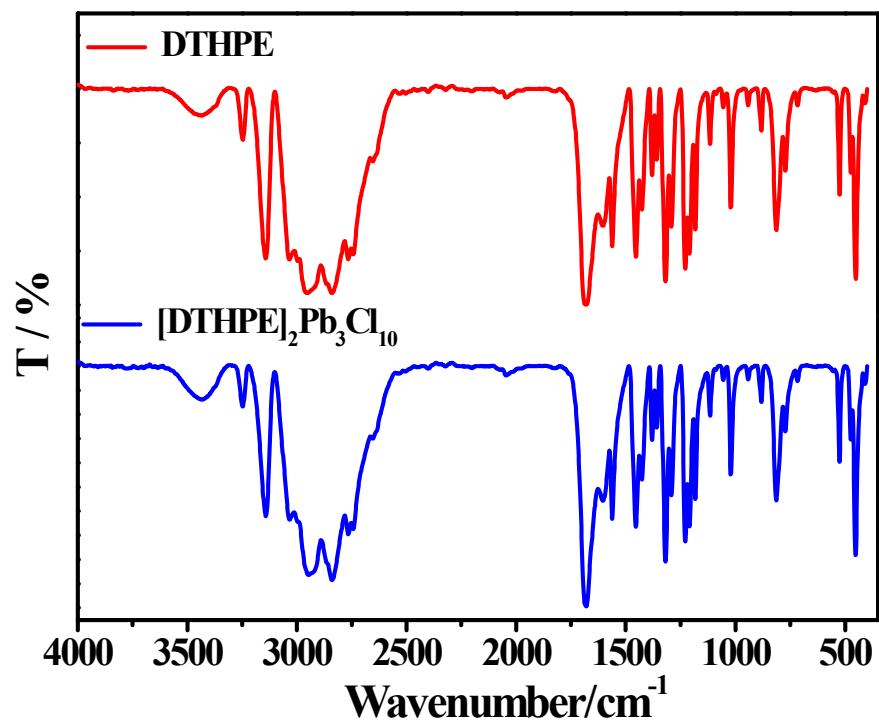
Fig. S16 The FT-IR spectra of DTHPE and [DTHPE]$_2$Pb$_3$Cl$_{10}$.

Table S1. Summarized distortion levels of $[PbX_6]$ octahedrons in compound $[DTHPE]_2Pb_3Cl_{10}$ and previously reported 2D perovskites.

Compound	$\Delta_{oct}\times10^{-4}$			Average	σ^2_{oct}			Average	Ref
	Pb1	Pb2	Pb3		Pb1	Pb2	Pb3		
$[DTHPE]_2Pb_3Cl_{10}$	7.33	9.70	—	8.52	113.69	96.94	—	105.32	This work
(epz)PbBr$_4$	77.37	18.04	18.75	38.05	46.08	33.63	35.41	38.37	3
(mpz)Pb$_3$Br$_{10}$	15.54	2.67	7.3	8.5	5.21	29.09	29.16	21.15	3
(4amp)PbBr$_4$	10.38	—	—	10.38	40.83	—	—	40.83	3
α-(DMEN)PbBr$_4$	30.8	4.0	—	17.4	25.84	8.87	—	17.36	4
(EDBE)PbBr$_4$	23.2	—	—	23.2	23.91	—	—	23.91	5
(BZA)$_2$PbCl$_4$	0.47	—	—	0.47	21.06	—	—	21.06	6
(2meptH$_2$)PbCl$_4$	0.14	—	—	0.14	4.09	—	—	4.09	7
(2meptH$_2$)PbBr$_4$	0.044	—	—	0.044	3.83	—	—	3.83	8
(C$_4$H$_9$NH$_3$)$_2$PbCl$_4$	0.043	—	—	0.043	9×10^{-4}	—	—	9×10^{-4}	9

* Analysis of octahedral distortion:

Bond length distortion:

$$\Delta d = \frac{1}{6}\sum\left[\frac{d_n - d}{d}\right]^2$$

in which d_n is the individual Pb-Cl bond length and d represents the average bond length.

Octahedral angle variance:

$$\sigma^2{}_{oct} = \frac{1}{11}\sum(a_i - 90)^2$$

The a_i represents the individual X-Pb-X angle. Δ_{oct} and $\sigma^2{}_{oct}$ represent bond distance and angle distortion levels, respectively.

Table S2. The PL performances of hybrid lead halides based on trimeric $[Pb_3X_{11}]^{5-}$ clusters.

Hybrid halides	Structure Type	CIE	PLQE	Lifetime	FWHM	Ref.
(bmpy)$_9$[Pb$_3$Br$_{11}$](MnBr$_4$)$_2$	0D cluster	(0.41,0.50)	15.7 %	27.43 ns	75 nm	10
		(0.29,0.65)	49.8 %	114.26μs	67 nm	
(bmpy)$_9$[ZnBr$_4$]$_2$[Pb$_3$Br$_{11}$]	0D cluster	(0.40, 0.53)	7 %	36 ns	68 nm	11
(bmpy)$_9$[ZnCl$_4$]$_2$[Pb$_3$Cl$_{11}$]	0D cluster	—	100 %	0.54 μs	61 nm	12
(bmpy)$_7$(PbCl$_4$)Pb$_3$Cl$_{11}$	0D cluster	(0.14, 0.19)	83 %	418 ns	84 nm	13
[DTHPE]$_2$Pb$_3$Cl$_{10}$	**1D chain**	**(0.25, 0.29)**	**19.45%**	**5.40 ns**	**174 nm**	**This work**

Table S3. Comparison of the broadband white light emission properties of $[DTHPE]_2Pb_3Cl_{10}$ and previously reported hybrid lead halides.

Hybrid halides	Structure Type	CIE	CRI	PLQE	Lifetime	Ref.
$Mn@(TDMP)PbBr_4$	1D perovskite	0.33, 0.36	96	60%	—	14
$(TDMP)PbBr_4$	1D perovskite	0.29, 0.37	75	45%	62 ns	15
$(C_4N_2H_{14})Pb_{0.992}Mn_{0.008}Br_4$	1D perovskite	0.37, 0.37	87	20-22%	28.2 ns	16
$(C_4N_2H_{14})PbBr_4$	1D perovskite	0.21, 0.28	63	18-20%	37.3 ns	17
$[DTHPE]_2Pb_3Cl_{10}$	**Non-perovskite 1D chain**	**0.25, 0.29**	**81**	**19.45%**	**5.40 ns**	**This work**

(PEA)$_2$PbBr$_3$Cl	2D perovskite	0.22, 0.21	90	16.9%	8.1 ns	18
(2,6-dmpz)$_3$Pb$_2$Br$_{10}$	Non-perovskite 1D chain	0.44, 0.46	77	12.24%	23.03ns	3
(BZA)$_2$PbBr$_2$Cl$_2$	2D perovskite	0.31,0.36	82	10.76%	7.58ns	6
(H$_2$O)(C$_6$H$_8$N$_3$)$_2$Pb$_2$Br$_8$Cl$_2$	1D perovskite	0.37, 0.44		10%	—	19
(EDBE)PbBr$_4$	2D perovskite	0.39, 0.42	84	9%	14 ns	5
(H$_2$O)(C$_6$H$_8$N$_3$)$_2$Pb$_2$Br$_{10}$	1D perovskite	0.41, 0.47		9%	54.14ns	19
(C$_6$H$_{13}$N$_4$)$_3$Pb$_2$Br$_7$	1D perovskite	0.42, 0.45		7%	106 ns	20
(BZA)$_2$PbCl$_4$	2D perovskite	0.28, 0.31	91	3.57	2.06ns	6
(2meptH$_2$)PbBr$_4$	2D perovskite	0.24, 0.23	91	3.37%	2.23 ns	8
(H$_2$DABCO)(Pb$_2$Cl$_6$)	Non-perovskite 3D framework	0.33, 0.34	96	2.5 %	1.98ns 54.13 ns	21
(EDBE)PbCl$_4$	2D perovskite	0.33, 0.39	81	2%	—	5
(2meptH$_2$)PbCl$_{1.4}$Br$_{2.6}$	2D perovskite	0.29, 0.33	86	1.67%	6.73 ns	7
(N-MEDA)PbBr$_{2.8}$Cl$_{1.2}$	2D perovskite	0.31, 0.36	82-85	1.5 %	1.2 ns	22
(2meptH$_2$)PbCl$_4$	2D perovskite	0.39, 0.44	84	1.05%	3.82 ns	7
(H$_3$O)(Et$_2$-DABCO)$_8$(Pb$_{21}$Cl$_{59}$)	Non-perovskite 3D framework	0.38,0.31	88	1 %	2.89 ns 18.85 ns	21
(C$_4$H$_9$NH$_3$)$_2$PbCl$_4$	2D perovskite	0.37, 0.40	86	1%	2.59 ns 9.68 ns	9
C$_5$H$_{14}$N$_2$PbCl$_4$·H$_2$O	1D perovskite	0.39, 0.37	93.9	1%	6.11 ns 5.6 ns	23
(epz)PbBr$_4$	2D perovskite	0.44, 0.44	84	0.97	2.7 ns	3

(hep)PbBr$_4$	1D perovskite	0.52, 0.41	89	0.63	4.3 ns	3
(4amp)PbBr$_4$	2D perovskite	0.31, 0.39	76	0.54	2.5 ns	3
(hmp) PbBr$_4$	3D perovskite	0.41, 0.39	90	0.46	2.5 ns	3
(hex)PbBr$_3$	1D perovskite	0.54, 0.40	88	0.35	—	3
(mpz)Pb$_3$Br$_{10}$	2D perovskite	0.38, 0.42	86	0.33	3.6 ns	3
(PEA)$_2$PbCl$_4$	2D perovskite	0.37, 0.42	84	—	4.2 ns	18
α-(DMEN)PbBr$_4$	2D perovskite	0.28, 0.36	73	—	1.39 ns	4
(CH$_3$CH$_2$NH$_3$)$_4$Pb$_3$Br$_{10-x}$Cl$_x$	2D perovskite	0.30, 0.35	83	—	1.21 ns	24

Table S4. The summarized parameters calculated from the theoretical fitting of temperature-dependent FWHM for hybrid lead halides.

Compound	Γ_0 (meV)	Γ_{phonon} (meV)	Γ_{inhomo} (meV)	E_{LO} (meV)	E_b (meV)	Ref
(H$_2$O)(C$_6$H$_8$N$_3$)$_2$Pb$_2$Br$_{10}$	419	150	49	18	14.5	19
(C$_4$H$_{14}$N$_2$)$_2$In$_2$Br$_{10}$	352±0.5	25	178	24.2	—	25
(2meptH$_2$)PbCl$_x$Br$_{4-x}$	580±2	88±3	157±12	12±3	32±1	7

[Pb$_2$X$_2$][O$_2$C(CH$_2$)$_4$CO$_2$]	494±9	49±3	72±5	13±2	19±3	26
[DTHPE]$_2$Pb$_3$Cl$_{10}$	**942.34**	**79.32**	**98.82**	**44.5**	**17.42**	**This work**

Table S5 Crystal Data and Structural Refinements for compound [DTHPE]$_2$Pb$_3$Cl$_{10}$.

chemical formula	$C_{20}N_8H_{44}Pb_3Cl_{10}$
fw	1372.70
Space group	$C2/c$ (No.15)
$a/Å$	20.069(3)
$b/Å$	11.785(2)
$c/Å$	16.398(3)
$\beta/^o$	97.014(2)
$V(Å^3)$	3849.4(11)
Z	4
D_{calcd} (g·cm^{-3})	2.369
Temp (K)	296(2)
μ (mm^{-1})	13.809
F (000)	2544
Reflections collected	22504
Unique reflections	4482
Reflections ($I>2\sigma(I)$)	3758
GOF on F^2	1.033
R_1, wR_2 ($I > 2\sigma(I)$)[a]	0.0244/ 0.0499
R_1, wR_2 (all data)	0.0339/ 0.0521

[a] $R_1 = \Sigma||F_0|-|F_c||/\Sigma|F_0|$, $wR_2 = [\Sigma(F_o^2 - F_c^2)/\Sigma w(F_0)^2]^{1/2}$

Table S6 Selected bond lengths (Å) for compound [DTHPE]$_2$Pb$_3$Cl$_{10}$.

Pb(1)-Cl(3)	2.7889(12)	Pb(2)-Cl(2)	2.7749(13)
Pb(1)-Cl(3)#1	2.7889(12)	Pb(2)-Cl(6)	2.8279(4)
Pb(1)-Cl(5)#1	2.9353(15)	Pb(2)-Cl(4)	2.8526(13)
Pb(1)-Cl(5)	2.9354(15)	Pb(2)-Cl(5)	2.9547(16)
Pb(1)-Cl(1)	2.9693(11)	Pb(2)-Cl(1)	2.9809(12)
Pb(1)-Cl(1)#1	2.9693(11)	Pb(2)-Cl(1)#1	3.0283(12)

Symmetry transformations used to generate equivalent atoms: #1 -x+1, y, -z+1/2.

Table S7 Selected bond angles (°) for compound [DTHPE]$_2$Pb$_3$Cl$_{10}$.

Cl(3)-Pb(1)-Cl(3)#1	107.86(6)	Cl(2)-Pb(2)-Cl(6)	101.72(3)
Cl(3)-Pb(1)-Cl(5)#1	98.90(4)	Cl(2)-Pb(2)-Cl(4)	97.62(3)
Cl(3)#1-Pb(1)-Cl(5)#1	97.76(4)	Cl(6)-Pb(2)-Cl(4)	95.97(2)
Cl(3)-Pb(1)-Cl(5)	97.76(4)	Cl(2)-Pb(2)-Cl(5)	96.29(4)
Cl(3)#1-Pb(1)-Cl(5)	98.90(4)	Cl(6)-Pb(2)-Cl(5)	103.66(3)
Cl(5)#1-Pb(1)-Cl(5)	151.51(6)	Cl(4)-Pb(2)-Cl(5)	153.03(4)
Cl(3)-Pb(1)-Cl(1)	165.10(4)	Cl(2)-Pb(2)-Cl(1)	88.24(3)
Cl(3)#1-Pb(1)-Cl(1)	86.74(4)	Cl(6)-Pb(2)-Cl(1)	169.98(2)
Cl(5)#1-Pb(1)-Cl(1)	81.59(4)	Cl(4)-Pb(2)-Cl(1)	81.45(3)
Cl(5)-Pb(1)-Cl(1)	76.47(4)	Cl(5)-Pb(2)-Cl(1)	76.00(4)

Cl(3)-Pb(1)-Cl(1)#1	86.74(4)	Cl(2)-Pb(2)-Cl(1)#1	166.00(3)
Cl(3)#1-Pb(1)-Cl(1)#1	165.10(4)	Cl(6)-Pb(2)-Cl(1)#1	92.28(2)
Cl(5)#1-Pb(1)-Cl(1)#1	76.47(4)	Cl(4)-Pb(2)-Cl(1)#1	80.63(3)
Cl(5)-Pb(1)-Cl(1)#1	81.59(4)	Cl(5)-Pb(2)-Cl(1)#1	80.30(3)
Cl(1)-Pb(1)-Cl(1)#1	78.87(4)	Cl(1)-Pb(2)-Cl(1)#1	77.76(3)

Symmetry transformations used to generate equivalent atoms: #1 -x+1, y, -z+1/2.

Table S8 Hydrogen bonds data for compound $[DTHPE]_2Pb_3Cl_{10}$.

D-H···A	d(D-H)	d(H···A)	d(D···A)	<(DHA)
N(3)-H(3C)···Cl(3)	0.86	2.39	3.2167	162
N(4)-H(4C)···Cl(2)	0.86	2.65	3.3640	142
C(1)-H(1A)···Cl(2)	0.93	2.61	3.5244	169
C(3)-H(3B)···Cl(3)	0.97	2.74	3.7050	171
C(5)-H(5A)···Cl(3)	0.97	2.75	3.7118	170
C(5)-H(5B)···Cl(1)	0.97	2.79	3.6035	142
C(7)-H(7B)···Cl(1)	0.97	2.83	3.7229	153

Reference

[1] G. M. Sheldrick, SHELXTL, University of Göttingen, Göttingen, **2001**.

[2] M. D. Segall, P. J. D. Lindan, M. J. Probert, C. J. Pickard, P. J. Hasnip, S. J. Clark and M. C. Payne, *J. Phys.: Condens. Matter.* **2002**, *14*, 2717-2744.

[3] L. L. Mao, P. J. Guo, M. Kepenekian, I. Hadar, C. Katan, J. Even, R. D. Schaller, C. C. Stoumpos and M. G. Kanatzidis, *J. Am. Chem. Soc.* 2018, **140**, 13078-13088.

[4] L. L. Mao, Y. L. Wu, C. C. Stoumpos, M. R Wasielewski and M. G. Kanatzidis, *J. Am. Chem. Soc.* 2017, **139**, 5210−5215.

[5] E. R. Dohner, A. Jaffe, L. R. Bradshaw and H. I. Karunadasa, *J. Am. Chem. Soc.* 2014, **136**, 13154-13157.

[6] M. H. Jung, *Inorg. Chem.* 2019, **58**, 6748-6757.

[7] S. S. Wang, Y. P. Yao, Z. Y. Wu, Y. Peng, L. N. Li and J. H. Luo, *J. Mater. Chem. C.* 2018, **6**, 4053.

[8] S. S. Wang, Y. P. Yao, J. T. Kong, S. G. Zhao, Z. H. Sun, Z. Y. Wu, L. N. Li and J. H. Luo, *Chem. Commun.* 2018, **54**, 4053.

[9] C. M. Ji, S. S. Wang, L. N. Li, Z. H. Sun, M. C. Hong and J. H. Luo, *Adv. Funct. Mater.* 2019, **29**, 1805038.

[10] M. Z. Li, J. Zhou, G. J. Zhou, M. S. Molokeev, J. Zhao, V. Morad, M. V. Kovalenko and Z. G. Xia, *Angew. Chem. Int. Ed.* 2019, **58**, 18670-18675.

[11] S. Lee, C. K. Zhou, J. Neu, D. Beery, A. Arcidiacono, M. Chaaban, H. R. Lin, A. Gaiser, B. H. Chen, T. E. Albrecht-Schmitt, T. Siegrist and B. W. Ma. *Chem. Mater.* 2020, **32**, 374-380.

[12] C. K. Zhou, H. R. Lin, J. Neu, Y. Zhou, M. Chaaban, S. Lee, M. Worku, B. H. Chen, R. Clark, W. H. Cheng, J. J. Guan, P. Djurovich, D. Z. Zhang, X. J. Lü, J. Bullock, C. Pak, M. Shatruk, M. H. Du, T. Siegrist and B. W. Ma, *ACS Energy Lett.* 2019, **4**, 1579−1583.

[13] C. K. Zhou, H. R. Lin, M. Worku, J. Neu, Y. Zhou, Y. Tian, S. Lee, P. Djurovich, T. Siegrist and B. W. Ma, *J. Am. Chem. Soc.* 2018, **140**, 13181−13184.

[14] H. L. Yuan, F. Massuyeau, N. Gautier, A. B. Kama, E. Faulques, F. Chen, Q. Shen, L. M. Zhang, M. Paris and R. Gautier, *Angew. Chem. Int. Ed.* 2020, **59**, 2802-2807.

[15] R. Gautier, F. Massuyeau, G. Galnon and M. Paris, *Adv. Mater*. 2019, **31**, 1807383.

[16] C. K. Zhou, Y. Tian, O. Khabou, M. Worku, Y. Zhou, J. Hurley, H. R. Lin and B. W. Ma, *ACS Appl. Mater. Interface.* 2017, **9**, 40446-40451.

[17] Z. Yuan, C. K. Zhou, Y. Tian, Y. Shu, J. Messier, J. C. Wang, L. J. van de Burgt, K. Kountouriotis, Y. Xin, E. Holt, K. Schanze, R. Clark, T. Siegrist and B. W. Ma, *Nat. Commun.* 2017, **8**, 14051.

[18] S. Yang, Z. H. Lin, J. W. Wang, Y. X. Chen, Z. D. Liu, E. Yang, J. Zhang and Q. D. Ling, *ACS Appl. Mater. Interfaces.* 2018, **10**, 15980−15987.

[19] A. Biswas, R. Bakthavatsalam, S. R. Shaikh, A. Shinde, A. Lohar, S. Jena, R. G. Gonnade and J. Kundu, *Chem. Mater.* 2019, **31**, 2253-2257.

[20] H. R. Lin, C. K. Zhou, Y. Tian, T. Besara, J. Neu, T. Siegrist, Y. Zhou, J. Bullock, K. S. Schanze, W. M. Ming, M. H. Du and B. W. Ma, *Chem. Sci.* 2017, **8**, 8400-8404.

[21] G. E. Wang, G. Xu, M. S. Wang, L. Z. Cai, W. H. Li and G. C. Guo, *Chem. Sci.* 2015. **6**. 7222-7226.

[22] E. R. Dohner, E. T. Hoke and H. I. Karunadasa, *J. Am. Chem. Soc.* 2014, **136**, 1718−1721.

[23] Y. Peng, Y. P. Yao, L. N. Li, Z. Y. Wu, S. S. Wang and J. H. Luo, *J. Mater. Chem. C.* 2018, **6**, 6033-6037.

[24] L. L. Mao, Y. L. Wu, C. C. Stoumpos, B. Traore, C. Katan, J. Even, M. R. Wasielewski and M. G. Kanatzidis, *J. Am. Chem. Soc.* 2017, **139**, 11956−11963.

[25] L. Zhou, J. F. Liao, Z. G. Huang, J. H. Wei, X. D. Wang, H. Y. Chen and D. B. Kuang, *Angew. Chem. Int. Ed.* 2019, **58**, 15435-15440.

[26] Z. W. Zhuang, C. D. Peng, G. Y. Zhang, H. M. Yang, J. L. Yin and H. H. Fei, *Angew. Chem. Int. Ed.* 2017, **56**, 14411-14416.